Power Electronics and Drives
Volume 9(44), 2024 DOI: 10.2478/pead-2024-0010

Power Electronics and Drives

Fault Tolerant Control of a Dual Star Induction Machine Drive System using Hybrid Fractional Controller

Research paper

Mokhtar Nesri[1,*], Hichem Benkadi[2], Kamal Nounou[3], Guedida Sifelislam[3], Mohamed Fouad Benkhoris[4]

[1]*Ecole Supérieur Ali Chabati, Reghaia Algiers, Algeria*
[2]*Ecole Supérieure des Techniques de l'Aéronautique (ESTA), Dar El Beida, Algiers, Algeria*
[3]*UER ELT, Ecole Militaire Polytechnique, 16111 Algiers, Algeria*
[4]*IREENA Laboratory Université de Nantes, Nantes, France*

Received: 19 December 2023; Accepted: 26 January 2024

Abstract: This paper presents a novel fault tolerant control (FTC) strategy for a dual star induction machine (DSIM) based on the combination of two types of robust controllers, namely a proportional resonant (PR) controller for current regulation and a fractional order PI (FOPI) for speed regulation. This FTC is associated with an indirect rotor indirect rotor field-oriented control (IRFOC) strategy. Fault feedforward compensation of the current components is introduced using the residual signal generated by the calculations passing through the PR controller. The fractional-order PI controller is applied as a feedforward fractional-order perturbation observer to the speed control loop, which attempts to minimise the error induced by the fault. In this context, a fault-tolerant control scheme is achieved. The performance characteristics of the proposed fault tolerant control for a dual star induction machine drive are compared with the fault tolerant control based on the conventional integer order IP (IOPI) to verify the effectiveness of the proposed FTC scheme under various conditions, by examining the robustness of the control in the presence of faults. To evaluate the performance of the proposed technique, simulation results are obtained using the Matlab/Simulink environment. According to the obtained simulation results, the proposed FTC system achieves significantly better responses than the conventional IRFOC system in terms of harmonics in the stator currents, and low oscillations in the electromagnetic torque response.

Keywords: *fault tolerance control • fractional order PI controller • dual star induction machine • proportional resonant controller • indirect rotor field-oriented control*

1. Introduction

The double star induction machine (DSIM) is a popular multiphase induction machine (MIM). It consists of two sets of three-phase windings with isolated neutral points and a phase shift of $\pi/6$ (Che et al., 2013a; Hadiouche, 2001). Many researchers are interested in controlling the performance and efficiency of DSIMs. The DSIM is considered to be an optimal choice in various applications that require high power, such as hybrid electric vehicles, rail traction and marine propulsion, as well as many other safety-critical applications such as embedded systems in avionics, marine or electric vehicles. Although DSIM is renowned for its low harmonic currents and torque pulsations, it offers multiple advantages, particularly in terms of power segmentation, reliability and increased efficiency (Badreddine et al., 2022).

The DSIM has a higher fault tolerance, allowing it to continue to operate and maintain its rotating flux even in the case of open-phase faults, due to the greater number of degrees of freedom that it has compared with three-phase machines. In the case of faults in the machine's phases in DSIM, the redundancy increases availability, since the

* *Email: nesri_m@yahoo.fr*

torque is produced by the healthy phases. Many researchers have focused increasingly on the design and control of DSIMs, to improve fault tolerance to achieve higher performance and efficiency (Duran et al., 2015).

In industry, the majority of faults are open-phase faults in one or more stator phases. Therefore, when an open phase fault is detected, fault tolerance control (FTC) should be applied immediately to ensure motor performance, safe operation and great economic benefits to the industry (Jiang and Yu, 2012).

Two main approaches have been observed in the literature concerning the (FTC): the first approach serves to maintain the elaborate model of the machine when it is healthy or considers a model of the asymmetrical machine having fewer phases. This approach relies on the calculation of new references of circulating current as a function of currents in $\alpha - \beta$ frame. This is to ensure the objective of the FTC (Che et al., 2013a; Duran et al., 2015). Although this approach is simple to implement, these new references often require the detection of the faulty phase and the use of an appropriate tabulation to impose the correct new references. The other method of control synthesis consists of using new reduced-order decoupling transformations to ensure constant stator variables in degraded mode (Bianchi et al., 2007).

As a result of this analysis, a new approach is envisaged to overcome the two methods set out in this paper. In reality, the complexity of the situations is due to the duality between adopting a new model or a new reference set, each of these being determined by the nature of the faults found. In response to this problem, a robust control technique is suggested to guarantee the system's insensitivity to closed-loop faults. This innovative approach maintains the same controller and the same structure, whatever the operational mode, whether normal or degraded. This approach, once designed, does not need to be adapted during operation. It has a simple structure and is not associated with controller-switching transients. Hence, the additional real-time computational demand is low. As this technique does not involve any switching, the behaviour of the system is much smoother than the techniques mentioned previously. Another benefit of this technique is that there is no need for a fault detection and diagnosis (FDD) unit, so there is no delay between the onset of a fault and the related control actions. The proposed DSIM control is fully engaged and control actions in the presence of a fault are always instantaneous.

In the absence of faults, because of simple control and good stability of PI controllers, they are widely used in DSIM control. As the current loop of DSIM control during a default set with classical PI regulator, it had to add a compensation to improve the dynamic performance, which leads to control structure complexity and a lack of robustness. Some references also designed robust control, for instance, a global efficiency optimisation of sliding mode control, a fuzzy logic control; a dynamic programming (DP) technology used to obtain an optimal solution. However, these control strategies such as DP algorithm are not suitable for real-time control; because they are based on a lot of data processing and a very low sample time (Wang et al., 2017).

Many controllers such as PIDs, fuzzy logic controllers and neural networks are used in DSIM speed control. Conventional PID controllers, though widely used for their simplicity, are inefficient in complex, non-linear, higher-order systems (Khurram et al., 2018).

The authors propose a proportional resonant (PR) regulator with indirect field-oriented control in order to obtain a best current tracking performance. For speed control, a fractional order PI (FOPI) controller is proposed due to better performance factors, such as robustness against system disturbances and parameter variations. It also contributes to better disturbance rejection control. The two controllers, FOPI speed and PR current controllers, are deployed in parallel with the PI speed and current controllers, respectively.

This paper presents a speed control strategy for a DSIM consisting of two types of controller, a PR current controller and a FOPI speed controller. A mathematical model design of the two controllers is presented in the following sections. Finally, the simulation results highlight the benefits of using the PR current controller and the FOPI speed controller in the DSIM drive system, through the significant reduction of undesirable harmonics.

The remainder of this paper is structured as follows: The modelling theory and principle of the DSIM IRFOC strategy are presented in Section 2, the current PR controller is detailed in Section 3, the speed fractional order PID (FOPID) controller is described in Section 4, and in Section 5 the simulation results are shown and discussed. Finally, Section 6 concludes the work.

2. Modelling and Control of DSIM

By neglecting magnetic saturation, mutual leakage inductance and core losses, and assuming a sinusoidal winding distribution, the DSIM model can be simplified (Hadiouche, 2001).

The DSIM can be considered as a hexaphase machine, and its equivalent model (in the α-β frame) can be obtained, from the natural model (*abc*) (Guedida et al., 2023), using the usual Concordia transformation matrix, denoted [T_6] (Hadiouche, 2001; Mohapatra et al., 2005), in order to make the variables of the machine constant in continuous regime. In fact, they are expressed in the rotating reference frame using the Park transformation matrix, denoted D (Gonzalez-Prieto et al., 2020).

After the Park transformation, the following relationships are obtained:

The voltage equations are given as follows:

$$\begin{cases} V_{sd} = R_s I_{sd} + \dfrac{d\varphi_{sd}}{dt} - \omega_s \varphi_{sq} \\ V_{sq} = R_s I_{sq} + \dfrac{d\varphi_{sq}}{dt} + \omega_s \varphi_{sd} \\ V_{sx} = R_s I_{sx} + \dfrac{d\varphi_{sx}}{dt} \\ V_{sy} = R_s I_{sy} + \dfrac{d\varphi_{sy}}{dt} \end{cases} \tag{1}$$

$$\begin{cases} V_{rd} = 0 = R_r I_{rd} + \dfrac{d\varphi_{rd}}{dt} - \omega_r \varphi_{rq} \\ V_{rq} = 0 = R_r I_{rq} + \dfrac{d\varphi_{rq}}{dt} + \omega_r \varphi_{rd} \end{cases} \tag{2}$$

The flux equations are given as follows:

$$\begin{cases} \varphi_{sd} = L_s I_{sd} + M I_{rd} \\ \varphi_{sq} = L_s I_{sq} + M I_{rq} \\ \varphi_{sx} = L_{ls} I_{sx} \\ \varphi_{sy} = L_{ls} I_{sy} \end{cases} \tag{3}$$

$$\begin{cases} \varphi_{rd} = L_r I_{rd} + M I_{sd} \\ \varphi_{rq} = L_r I_{rq} + M I_{sq} \end{cases} \tag{4}$$

The electromagnetic torque equation is given as follows:

$$T_{em} = p\frac{M}{L_r}\left(\varphi_{rd} I_{sq} - \varphi_{rq} I_{sd}\right) \tag{5}$$

The different electrical angles are linked by the relationship:

$$\theta_s = \theta_m + \theta_r \tag{6}$$

The mechanical equation is written as follows:

$$J\frac{d\Omega}{dt} = T_{em} - T_L - k_f \Omega \tag{7}$$

With: $\omega_s = \dot{\theta}_s$: is the stator pulsation, $\omega_r = \dot{\theta}_r$: is the rotor pulsation, $\omega_m = \omega_s - \omega_r = \dot{\theta}_m = p\Omega$: is the mechanical pulsation, *p*: is the number of pairs of poles.

2.1. Indirect rotor field-oriented control (IRFOC) strategy

By orienting the *d–q* axis system in such a direction that the *d* axis is in phase with the rotor flux:

$$\begin{cases} \varphi_{rq} = 0 \\ \varphi_{rd} = \varphi_r \end{cases} \tag{8}$$

By substituting Eq. (8) in Eq. (4) and after development, the rotor flux expression can be written as follows:

$$\varphi_r = L_r I_{rd} + M I_{sd} \tag{9}$$

And by substituting Eq. (8) in Eq. (4) and after development, the current component I_{rd} expression becomes:

$$I_{rd} = -\frac{1}{R_r}\frac{d\varphi_r}{dt} \tag{10}$$

By substituting Eq. (10) in Eq. (4) and after development, the rotor flux expression can be written as:

$$\varphi_r + \frac{L_r}{R_r}\frac{d\varphi_r}{dt} = M I_{sd} \tag{11}$$

By applying the Laplace transformation to the Eq. (11), the rotor flux expression becomes:

$$\varphi_r = \frac{M}{1 + T_r s} I_{sd} \tag{12}$$

In the permanent regime the rotor flux expression becomes as follows:

$$\varphi_r = M I_{sd} \tag{13}$$

The electromagnetic torque Eq. (5) can be written as follows:

$$T_{em} = p\frac{M}{L_r}\varphi_r I_{sq} \tag{14}$$

From the rotor voltage equations Eq. (2), we can deduce the equation (ω_r) which is deduced as a function of the stator currents I_{sd}, I_{sq} and the rotor time constant $T_r = L_r/R_r$ and is as follows:

$$\omega_r = \frac{1}{T_r}\frac{I_{sq}}{I_{sd}} \tag{15}$$

The DSIM indirect rotor flow orientation control (IRFOC) scheme can be deduced and illustrated as shown in Figure 1.

In the field-oriented control, the stator current is decomposed into two components namely direct axis component (I_{ds}) and quadrature axis component (I_{qs}). The direct axis component is in the direction of flux linkage, and the quadrature axis component is orthogonal to it. The fast dynamics of the response of the motor can be achieved as both the components of the current are controlled individually and independently. An induction motor needs only these current components of current for torque generation, regardless of the number of phases. It should be noted that, in the range of speeds under the nominal speed of the machine, the d-axis current is kept constant, whereas operating in over-speed mode requires a defluxing which then requires an appropriate reduction of this current component.

The general structure of the pre-fault control strategy is shown in Figure 1. The scheme is an indirect rotor field oriented control (IRFOC) with an outer speed control loop and inner current control loops for *d–q, x–y*. Four phase currents need to be measured in the two/single neutral configurations because the remaining phase currents can be obtained from the condition of having two/one isolated neutral points. The measured phase currents are converted into $\alpha - \beta$ currents frame using the Concordia transformation [T_6] (Duran et al., 2015) and *d–q* currents are obtained from the rotation of $\alpha - \beta$ currents frame in the forward (synchronous) direction using the Park transformation.

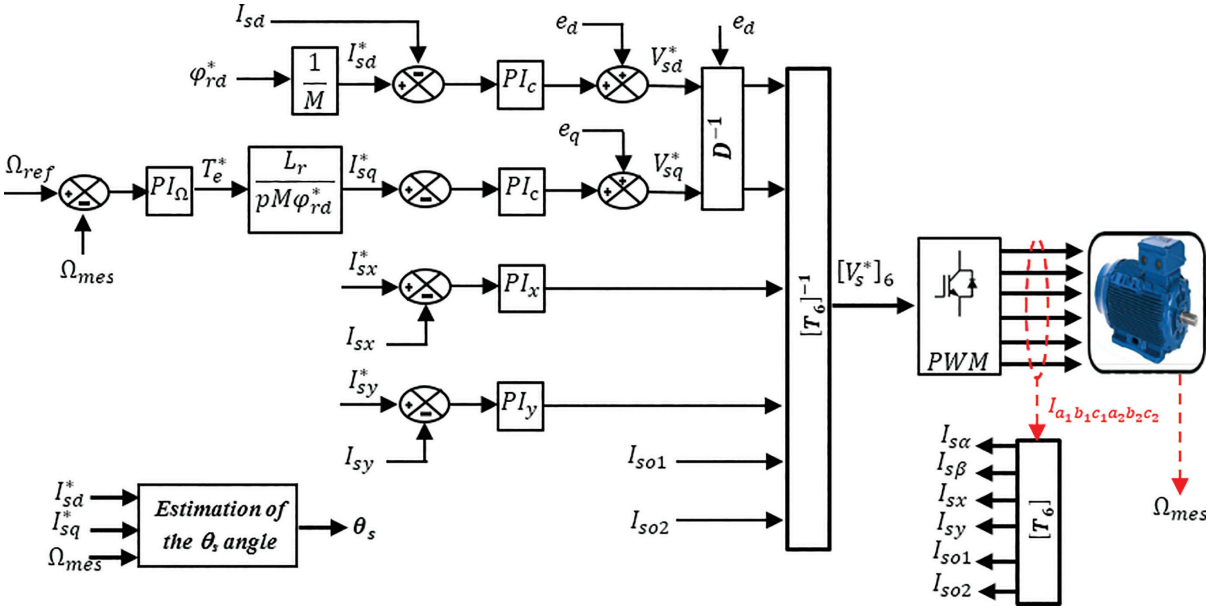

Fig. 1. IRFOC Schematic block diagram of DSIM drive.

3. PR Controller

Sato et al. (1998) introduced the PR controller which provided a fairly simple and attractive solution in the case of *abc*-natural or $\alpha-\beta$-stationary reference systems. Compared with the conventional PI controller, it can overcome two well-known drawbacks of the latter: poor disturbance rejection capability and the inability to track a sinusoidal reference with zero steady-state error. Generally speaking, we can conclude that the resonance term has a direct impact on the transient process but does not modify the root diagram (Tafti et al., 2014; Teodorescu et al., 2006), while the proportional term has a direct impact on the stability domain. It was demonstrated that the cut-off frequency of the damping term increases the stability domain but can be a reason for the steady-state error (Husev et al., 2019; Ye et al., 2016; Zmood and Holmes, 2003).

A classic PI controller is often used to control electrical machines, because it is easy to identify its parameters and is efficient in its mission. In the case of polyphase machines, the appearance of a stator phase cut-off fault causes a non-sinusoidal magnetic field, which in turn leads to the appearance of harmonics in the stator current, resulting in torque and speed ripples.

$$C_{PI}(s) = k_p \frac{1+\tau_i s}{\tau_i s} \tag{16}$$

In the above equation, C_{PI} Is the transfer function of a conventional PI controller, k_p is the proportional gain and τ_i is the integral time constant.

The effectiveness of the conventional PI regulator in reducing current ripples in the presence of disturbing harmonics depends on its frequency response. This corrector is characterised by infinite gain in the static regime, i.e. at $f = 0$, and finite gain (k_p) at high frequencies (Figure 2). The progressive decrease in gain in the passband, i.e. for frequencies from 0 to $f_0 = \omega_0/2\pi$. Effectively attenuates variable disturbances below the cut-off frequency f_0 without, however, cancelling them out completely, but does not modify them outside the passband, when the frequency of disturbances exceeds f_0.

We now assume that the current set point remains constant. In degraded operation, harmonic voltages disturb I_{sdq} currents. In this situation, the static error is no longer zero, as the PI corrector can only reject constant disturbances. Harmonics are therefore superimposed on the continuity component of normal operation. In summary, the PI controller perfectly preserves the continuous component of references applied to servo-controls. This makes it particularly suitable for tracking current set points in steady-state operation. To improve torque ripple reduction,

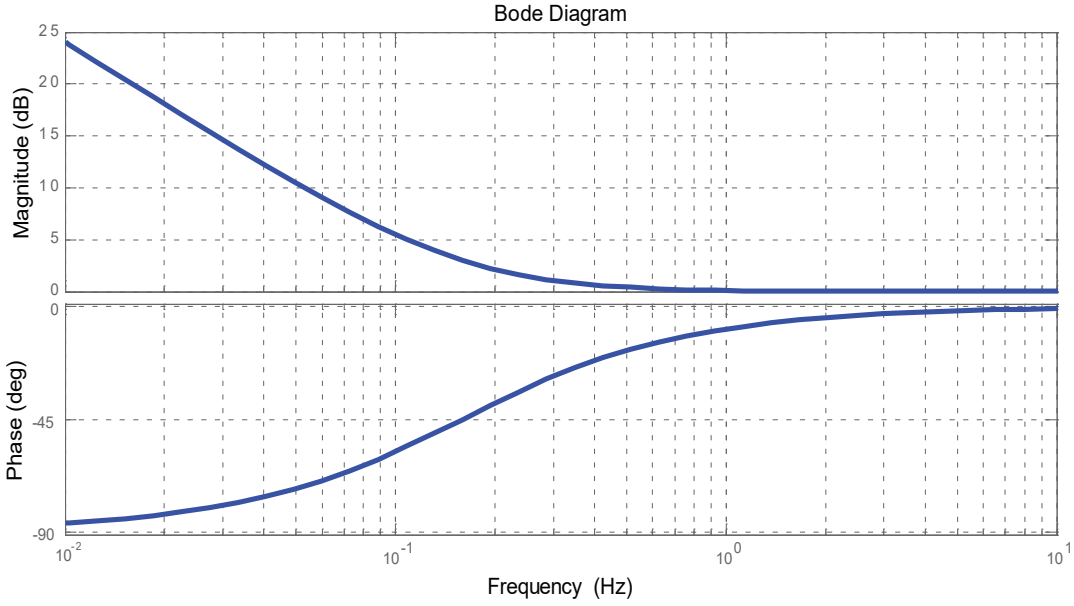

Fig. 2. Bode diagrams of a PI controller ($k_p = 1$ et $\tau_i = 1$).

we need to consider a corrector based on the properties of the PI at zero frequency, but transposed to disturbance frequencies.

Inserting this corrector into a current loop with a 1st-order RL circuit does not change the class of the transfer function. This observation helps us to construct the transfer function of the desired corrector using that of the PI given by relation (16). Based on the frequency transposition proposed in Crévits, (2010), Naslin (1968) and Salimin et al. (2019), we use the following change of variable:

$$s \rightarrow \frac{1}{2}\frac{s^2+\omega_c^2}{s} \tag{17}$$

with $\omega_c = 2\pi f_c$ is the pulsation to be rejected.

Applying this change of variable allows us to establish the transfer function of the PR controller:

$$C_{PR}(s) = k_p \frac{1+\tau_i\left(\frac{1}{2}\frac{s^2+\omega_c^2}{s}\right)}{\tau_i\left(\frac{1}{2}\frac{s^2+\omega_c^2}{s}\right)} \tag{18}$$

$$C_{PR}(s) = k_p \frac{s^2+\frac{2}{\tau_i}s+\omega_c^2}{s^2+\omega_c^2} \tag{19}$$

The transfer function (19) is that of a selective filter at pulsation ω_c which will take effect in a resonant corrector.

Figure 3 shows the Bode diagrams of this transfer function Eq.(19). The very high gain at resonance frequency f_c, is clearly visible.

The transfer function of the mono-frequency resonant corrector is given in the following general form (Wulveryck, 2000):

$$C_{PR}(s) = \frac{b_2 s^2 + b_1 s + b_0}{s^2 + (h\omega_c)^2} = K + \frac{b_1 s + b_0}{s^2 + (h\omega_c)^2} \tag{20}$$

where ω_c is the fundamental pulsation and h is the order of the harmonic to be rejected. The coefficients b_i characterise the response of the corrector. The static gain K is derived from the decomposition into simple elements of the initial form Eq. (20).

There are several types of PR controllers. An ideal PR Controller form with an infinite gain at ω_{c_h} is given as (Husev et al., 2019):

$$C_{PRC}^{\text{ideal}}(s) = K_p + \sum_{h=1,3,5,7\ldots} k_{rh} \frac{s}{s^2 + \omega_{c\_h}{}^2} \tag{21}$$

Following this strategy, restoring a constant torque invites us to eliminate harmonic current disturbances by assisting the natural filtering effect of PI correctors with that of resonant correctors acting on previously identified frequencies.

The current control devices, extracted from the IRFOC schematic block diagram of DSIM drive in Figure 1, are represented for a one-phase machine axis by the block diagram in Figure 4 (Che et al., 2013b; Husev et al., 2019). The system is a winding of the machine (type RL, order 1) commonly modelled by a first-order transfer function:

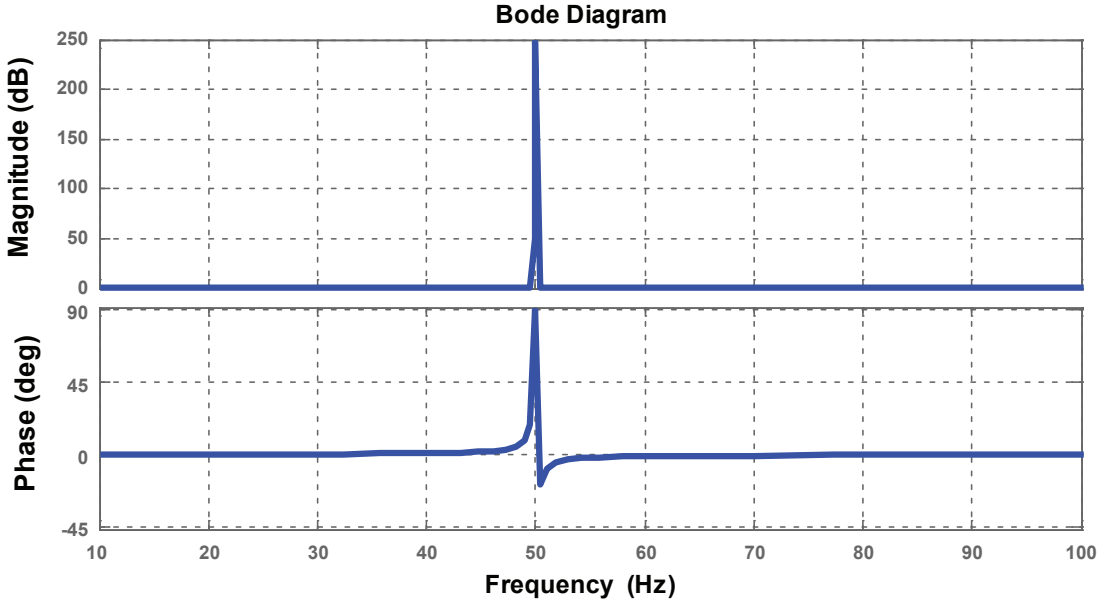

Fig. 3. Bode diagrams of a PR controller (k_p = 1, τ_i = 1 et f_c = 50*Hz*).

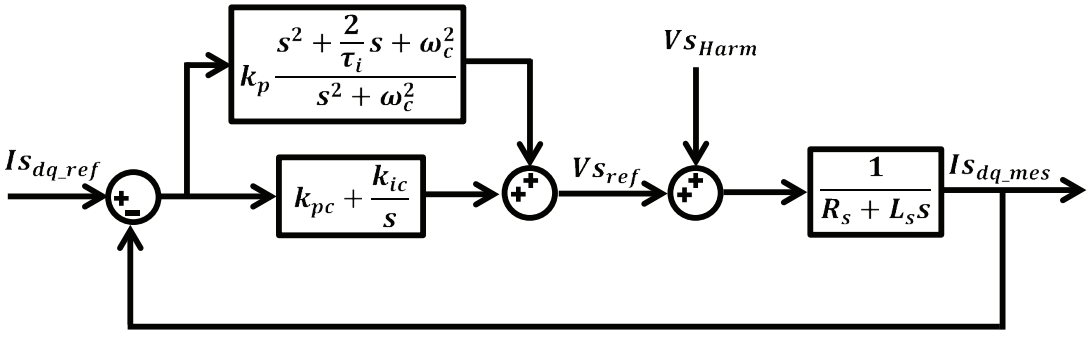

Fig. 4. Representation of the stator current control loop.

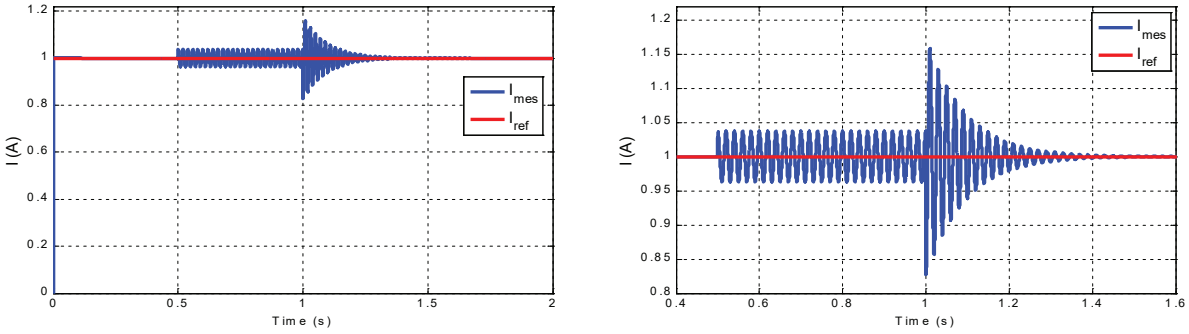

(a) Current curves (a') Current curves (Zoom)

Fig. 5. Response of the current loop with a PR controller (f_c = 50*Hz*).

For testing and evaluating the effectiveness of the PR controller, refer to Figure 5 which shows the result of the simulation of the current response in the various situations indicated, in order to decompose the different actions of the PR controller. The PR controller has a resonance frequency of 50 Hz. The response initially illustrates the application of the undisturbed current set point. The latter, which includes a 50 Hz harmonic, appears at t = 0.5 s. It is initially processed only by the conventional PI controller (from 0.5 to 1 s). The conventional PI controller is unable to reject ripples. As soon as the resonant part of the corrector is activated (at t = 1 s), the disturbances are immediately rejected. The application of this approach to a real machine is the subject of the next section.

4. FOPID Controller

The FOPID controller (or $PI^{\mu}D^{\lambda}$) was firstly proposed by Podlubny in 1999 (Podlubny, 1999a), as an extended version of the conventional integer order PID (IOPID). Based on the fractional calculus, the FOPID controller is characterised by five parameters: proportional gain (k_p), integration gain (k_i), derivative gain (k_d), integration order (μ) and derivative order (λ) (Podlubny, 1999b). Fractional integral and derivative provide flexibility in the tuning strategy of PID controllers and better-shaped closed-loop responses to achieve more satisfactory results (Rahimian and Tavazoei, 2012; Zhao et al., 2018).

One of the most important advantages of the FOPID corrector is its potential to control the dynamics of fractional-order systems effectively. Another advantage lies in the fact that FOPID correctors are less sensitive to changes in the parameters of a controlled system, resulting in improved robustness.

The standard PID controller is defined in series (interacting) form as:

$$C_{PID}(s) = k_p + \frac{k_i}{s} + k_d s \tag{22}$$

where k_p is the proportional gain, k_i is the integral gain and, k_d is the derivative gain.

The FOPID controller is defined as a generalisation of the standard PID controller Eq. (22), namely,

$$C_{FOPID}(s) = k_p + \frac{k_i}{s^{\mu}} + k_d s^{\lambda} \tag{23}$$

where μ and λ are the non-integer orders of the integral and derivative terms respectively.

4.1. Approximation by a rational function of the FOPID controller

The implementation of fractional-order correctors requires the replacement of fractional-order transfer functions by integer-order transfer functions with a behaviour similar to that desired, but much more easily manipulated. There are several methods for approximating such functions (de Oliveira Valério, 2005; Petras et al., 2002).

Indeed, in order to implement the fractional-order controller, the Oustaloup continuous integer-order approximation (Oustaloup et al., 1996) has been employed. It consists in using the following approximation based on a recursive distribution of zeros and poles:

$$s^{\alpha} \cong k\prod_{n=1}^{N}\frac{1+\dfrac{s}{\omega_{z,n}}}{1+\dfrac{s}{\omega_{p,n}}},\ \alpha>0 \tag{24}$$

which is valid in a frequency range $[\omega_l,\omega_h]$ and where the gain k is adjusted so that the right side of Eq. (6) has unity gain al the gain crossover frequency of s^{α}.

Where ω_l and ω_h are the high and low transitional frequencies respectively. Using the described Oustaloup-Recursive-Approximation (ORA) method with:

$$\omega_l=10^{-2},\omega_h=10^{+2}$$

the obtained approximation for fractional function $g(s)=\dfrac{1}{s^{0.5}}$ is:

$$\widehat{g_{0.5}}(s)=\frac{0.1s^5+7.497s^4+76.85s^3+121.8s^2+29.85s+1}{s^5+29.85s^4+121.8s^3+76.85s^2+7.497s+0.1} \tag{25}$$

Figure 6 shows the Characteristics of approximated fractional order integrator of Eq. (21) for μ=0.5 and N = 5: and Bode diagrams of this transfer function.

Figure 7 shows the speed control loop which was extracted from the IRFOC schematic block diagram of DSIM drive in Figure 1. The relationship Eq. (7) was modeled by a first-order transfer function (type RL, order 1).

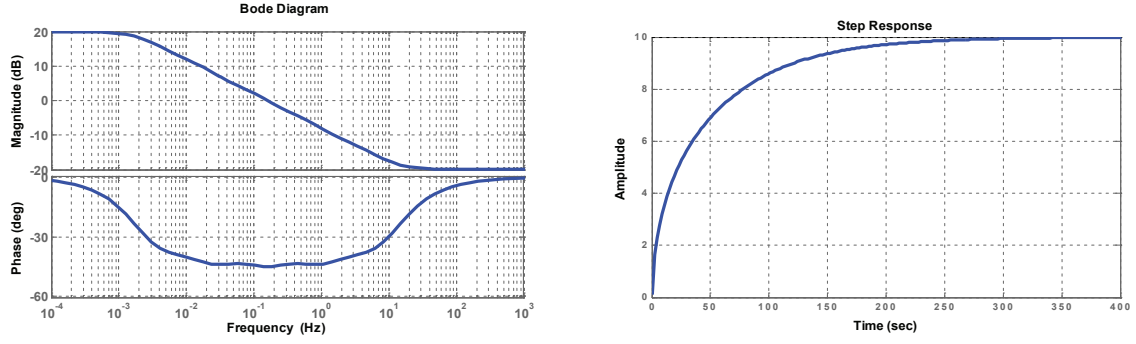

Fig. 6. Characteristics of approximated fractional order integrator Eq. (21) for μ=0.5 and N = 5: Bode plots (left), Unit step response (right).

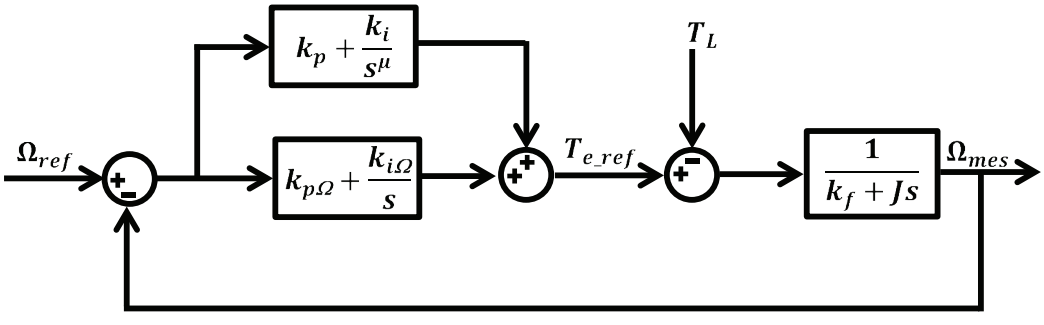

Fig. 7. Diagram of the speed control loop.

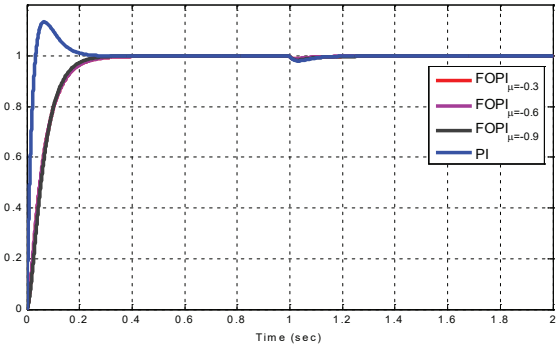

(a) Speed curves

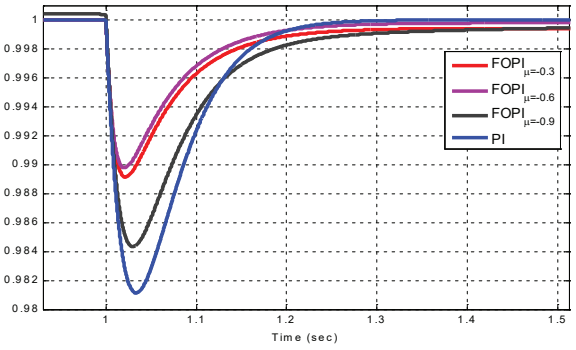

(a') Speed curves (Zoom)

Fig. 8. Indicial responses of speed closed loop: *PI*,$FOPI_{\mu = 0.3,\ 0.6,\ 0.9}$

Figure 8 shows the speed closed-loop indicial responses (Figure 7) for the integer-order PI (IOPI) controller and the FOPI controller for $\mu = 0.3, 0.6, 0.9$. A torque load is applied at $t = 1s$,we can observe that the $FOPI_{\mu=0.6}$ controller has improved the system's indicial response considerably in terms of overshoot, response time, and in terms of disturbance rejection duration.

5. Simulation results

In order to verify the study carried out, the model of the DSIM with two isolated neutrals and its control (IRFOC) in degraded mode have been implemented, under the Simulink environment of the MATLAB software, the parameters of the simulated machine are shown in the Appendix. To test the effectiveness of the proposed method, a most critical fault scenario (opening of two adjacent stator phases a_1 and a_2) will be performed.

The machine turns at a fixed speed of 50rad/s without load. At time t = 1s, a load torque equal to 10 Nm is applied, and at time t = 2 s, the opening fault of two phases (a_1 and a_2) is provoked; and at time t = 3s, the resonant regulator in the current loop and the fractional regulator in the speed loop are activated.

The opening fault in phases a_1 and a_2 of the machine causes the appearance of ripples in the *d-q* currents, as a result of the disequilibrium created, and these ripples in the *d-q* currents produces a significant ripple in the speed and electromagnetic torque, which will be very severe in the time length of the conventional PI controller, but practically negligible within the application interval of the fractional and resonant controller hybridisation. The simulation results are shown in Figure 9.

Figure 10 shows the Fast Fourier Transform (FFT) of the current I_{c1} during the three operating modes (pre-fault mode (a), degraded mode (b) and degraded mode with the proposed control (c)). It should be noted that the switching frequency is of the order of 8 kHz. As the current does not have the same amplitude for each time interval, we divided by the amplitude of the fundamental to obtain the units in per unit and compared the results. We can clearly see that the amplitudes of the current spectrum during the activation of the resonant regulator in the current loop and the fractional regulator in the speed loop are lower than those when the controllers are not activated (t< 3 s), hence we have an improvement in the harmonic content.

The Figure 11 represents the spectrum analysis of the electromagnetic torque before, during, and after the degraded mode operation and the activation of the proposed FTC method. It can be seen that the amplitudes of the components of the electromagnetic torque spectrum increase significantly when the fault is applied. However, when the proposed FTC method is activated, the amplitudes of the harmonics are significantly attenuated, thus indicating an improvement in the harmonic content of the torque. This implies smoother torque and reduced machine vibration.

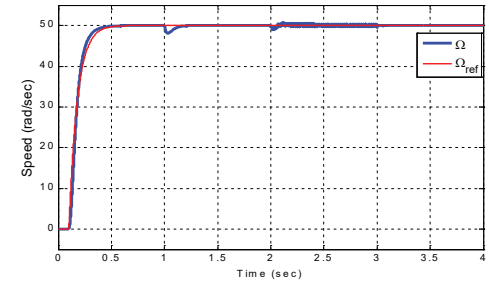

(a) Speed curves

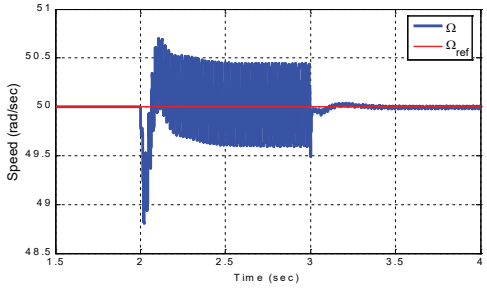

(a') Speed curves (Zoom)

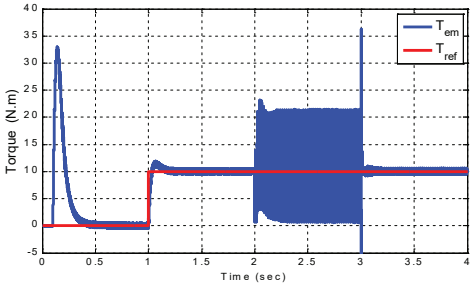

(b) Electromagnetic torque curves.

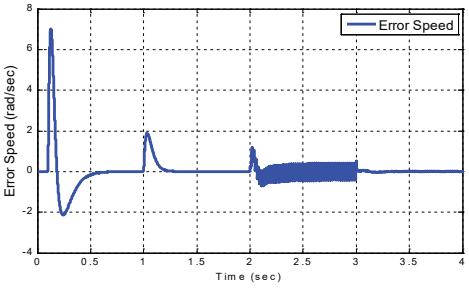

(a'') Speed error curves.

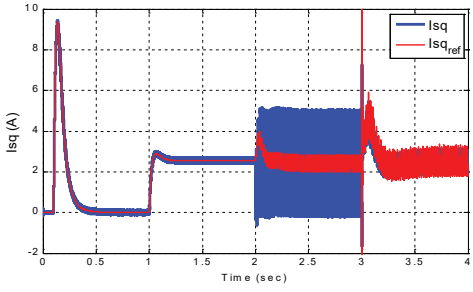

(c) Star currents (Isq) components curves

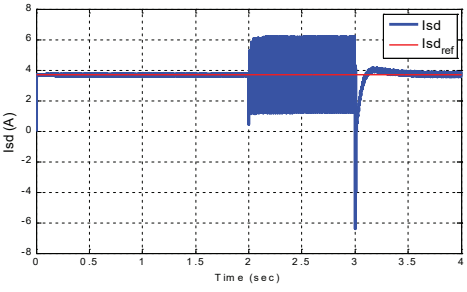

(d) Star currents (Isd) components curves

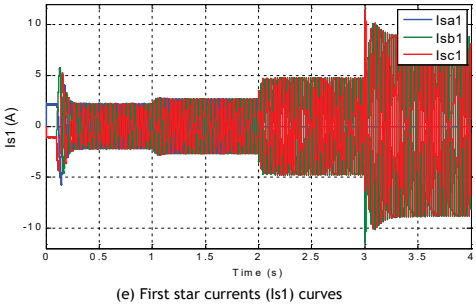

(e) First star currents (Is1) curves

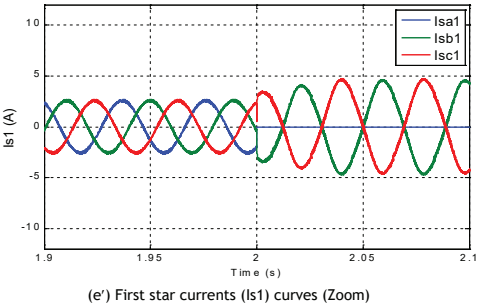

(e') First star currents (Is1) curves (Zoom)

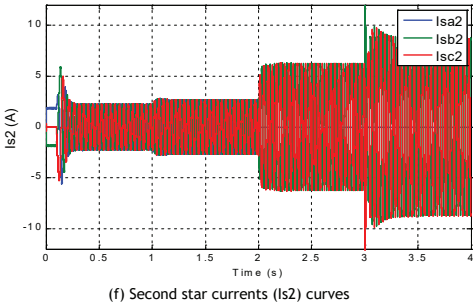

(f) Second star currents (Is2) curves

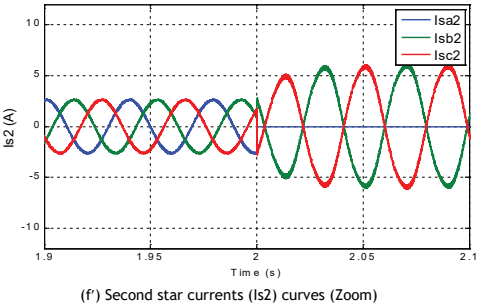

(f') Second star currents (Is2) curves (Zoom)

Fig. 9. DSIM IRFOC and HFBC simulations results.

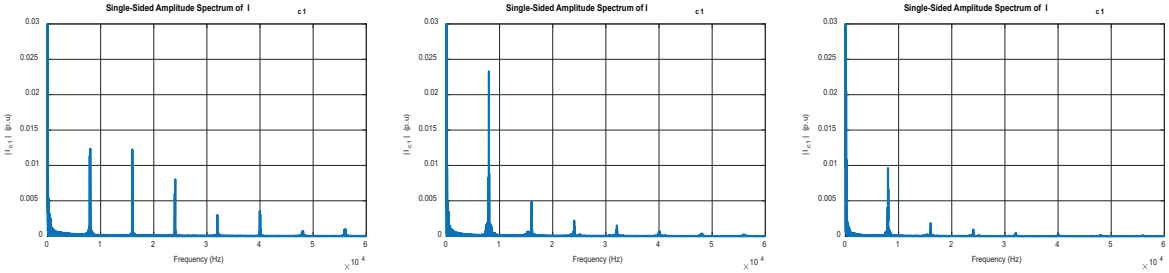

(a) FFT of currents (Ic1) during pre-fault mode and without proposed method

(b) FFT of current (Ic1) during degraded mode and without proposed method

(c) FFT of current (Ic1) during degraded mode and during proposed FTC activation

Fig. 10. Current phase-Ic1 spectrum analysis.

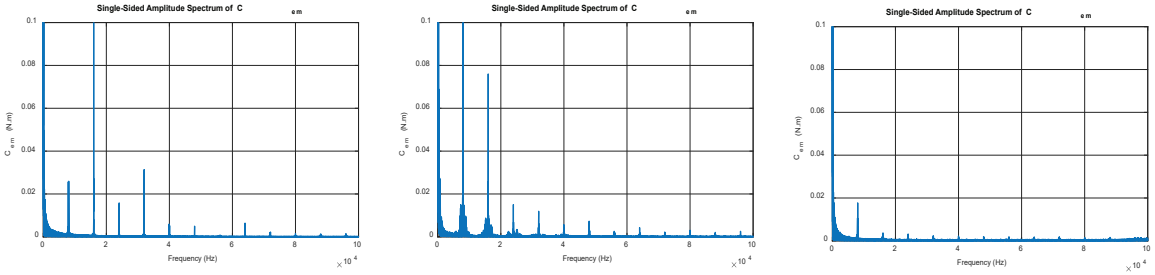

(a) FFT of electromagnetic torque during pre-fault mode and without proposed method

(b) FFT of electromagnetic torque during degraded mode and without proposed method

(c) FFT of electromagnetic torque during degraded mode and during proposed FTC activation

Fig. 11. DSIM IRFOC and HFBC simulations results of FFT spectrum of electromagnetic torque.

6. Conclusion

We proposed a hybrid FOPI controller and PR controller to design a fault tolerance control (FTC) of a dual star induction machine (DSIM) drive under Indirect rotor field-oriented control (IRFOC) strategy. The proposed FTC scheme (IRFOC with FOPI+PR controllers) provides the better responses compared to the conventional IRFOC scheme (IRFOC with IOPI). The effectiveness of these architectures (IRFOC with FOPI+PR controllers) has been demonstrated by examples of simulation of opening of two adjacent stator phases and satisfactory results were obtained. In this paper, fractional calculus and PR controller have been briefly described. From simulation results, it was verified that even though the proposed PR-type current control algorithm is simple and easy to implement with the proposed speed controller, it yields good control performance in the event of fault.

References

Badreddine, L., Fouad, B. and Samir, Z. (2022). Modelling and control of double star induction machine used active fault tolerant control based on backstepping controller and nonlinear adaptive observer. In: 2022 International Conference of Advanced Technology in Electronic and Electrical Engineering (ICATEEE). M'sila: Algeria, pp. 1–6.

Bianchi, N., Bolognani, S. and Dai Pré, M. (2007). Strategies for the Fault-Tolerant Current Control of a Five-Phase Permanent-Magnet Motor. IEEE Transactions on Industry Applications, 43(4), pp. 960–970. doi: 10.1109/TIA.2007.900445.

Che, H. S., Duran, M. J., Levi, E., Jones, M., Hew, W.-P. and Rahim, N. A. (2013a). Postfault Operation of an Asymmetrical Six-Phase Induction Machine with Single and Two Isolated Neutral Points. IEEE Transactions on Industrial Electronics, 29(10), pp. 5406–5416. doi: 10.1109/TPEL.2013.2293195.

Che, H. S., Levi, E., Jones, M., Hew, W.-P. and Rahim, N. A. (2013b). Current Control Methods for an

Asymmetrical Six-Phase Induction Motor Drive. IEEE Transactions on Power Electronics, 29(1), pp. 407–417. doi: 10.1109/TPEL.2013.2248170.

Crévits, Y., “Caractérisation et commande des entraînements polyphasés en mode dégradé d’alimentation”, Thèse de doctorat, Université des Sciences et Technologies de Lille 1,12 juillet 2010

de Oliveira Valério, D. P. M. (2005). Fractional Robust System Control,” Ph.D. thesis. Inst. Super. Técnico, Univ. Técnica Lisboa.

Duran, M. J., Prieto, I. G., Bermudez, M., Barrero, F., Guzman, H. and Arahal, M. R. (2015). Optimal Fault-Tolerant Control of Six-Phase Induction Motor Drives with Parallel Converters. IEEE Transactions on Industrial Electronics, 63(1), pp. 629–640. doi: 10.1109/TIE.2015.2461516.

Gonzalez-Prieto, A., Aciego, J. J., Gonzalez-Prieto, I. and Duran, M. J. (2020). Automatic Fault-Tolerant Control of Multiphase Induction Machines: A Game Changer. Electronics, 9(6), p. 938. doi: 10.3390/electronics9060938.

Guedida, S., Tabbache, B., Nounou, K. and Benbouzid, M. (2023). Direct Torque Control Scheme for Less Harmonic Currents and Torque Ripples for Dual Star Induction Motor. Revue Roumaine des Sciences Techniques, Série Électrotechnique et Énergétique, 68(4), pp. 331–338. doi: 10.59277/RRST-EE.2023.4.2.

Hadiouche, D. (2001). Contribution à l’étude de la machine asynchrone double étoile: modélisation, alimentation et structure. Nancy, p. 1.

Husev, O., Roncero-Clemente, C., Makovenko, E., Pimentel, S. P., Vinnikov, D. and Martins, J. (2019). Optimization and Implementation of the Proportional-Resonant Controller for Grid-Connected Inverter with Significant Computation Delay. IEEE Transactions on Industrial Electronics, 67(2), pp. 1201–1211. doi: 10.1109/TIE.2019.2898616.

Jiang, J. and Yu, X. (2012). Fault-Tolerant Control Systems: A Comparative Study Between Active and Passive Approaches. Annual Reviews in Control, 36(1), pp. 60–72. doi: 10.1016/j.arcontrol.2012.03.005.

Khurram, A., Rehman, H., Mukhopadhyay, S. and Ali, D. (2018). Comparative Analysis of Integer-Order and Fractional-Order Proportional Integral Speed Controllers for Induction Motor Drive Systems. Journal of Power Electronics, 18(3), pp. 723–735. doi: 10.6113/JPE.2018.18.3.723.

Mohapatra, K. K., Kanchan, R. S., Baiju, M. R., Tekwani, P. N. and Gopakumar, K. (2005). Independent Field-Oriented Control of Two Split-Phase Induction Motors From a Single Six-Phase Inverter. IEEE Transactions on Industrial Electronics, 52(5), pp. 1372–1382. doi: 10.1109/TIE.2005.855659.

Naslin, P. (1968). “Technologie et calcul pratique des systèmes asservis,”, 3 ed. Dunod.

Oustaloup, A., Moreau, X. and Nouillant, M. (1996). The CRONE Suspension. Control Engineering Practice, 4(8), pp. 1101–1108. doi: 10.1016/0967-0661(96)00109-8.

Petras, I., Podlubny, I., O’Leary, P., Dorack, L’ and Vinagre, B. M. (2002). Analogue Realisations Of Fractional Order Controllers. TU Koosice: Faculta Berg.

Podlubny, I. (1999a). Fractional-Order System and PI α D β Controller. IEEE Transactions on Automatic Control, 44, pp. 208–214, DOI: 10.1109/9.739144.

Podlubny, I. (1999b). Fractional-Order Systems and PI/Sup/Spl Lambda//D/Sup/Spl mu//-Controllers. IEEE Transactions on Automatic Control, 44(1), pp. 208–214. doi: 10.1109/9.739144.

Rahimian, M. A. and Tavazoei, M. S. (2012). Application of Stability Region Centroids in Robust PI Stabilization of a Class of Second-Order Systems. Transactions of the Institute of Measurement and Control, 34(4), pp. 487–498. doi: 10.1177/0142331211400117.

Salimin, S., Noor, A. F. M. and Jumaat, S. A. (2019). Proportional Resonant Current Controller Strategy in Inverter Application. International Journal of Power Electronics and Drive Systems, 10(4), p. 2238.

Sato, Y., Ishizuka, T., Nezu, K. and Kataoka, T. (1998). A New Control Strategy for Voltage-Type PWM Rectifiers to Realize Zero Steady-State Control Error in Input Current. IEEE Transactions on Industry Applications, 34(3), pp. 480–486. doi: 10.1109/28.673717.

Tafti, H. D., Maswood, A. I., Ukil, A., Gabriel, O. H. P. and Ziyou, L. (2014). NPC photovoltaic grid-connected inverter using proportional-resonant controller. In: 2014 IEEE PES Asia-Pacific Power and Energy Engineering Conference (APPEEC). Hong Kong: China, pp. 1–6.

Teodorescu, R., Blaabjerg, F., Liserre, M. and Loh, P. C. (2006). Proportional-Resonant Controllers and Filters for Grid-Connected Voltage-Source Converters. EE Proceedings - Electric Power Applications, 153(5), pp. 750–762. doi: 10.1049/ip-epa:20060008.

Wang, X., Lv, H., Sun, Q., Mi, Y. and Gao, P. (2017). A Proportional Resonant Control Strategy for Efficiency Improvement In Extended Range

Electric Vehicles. Energies, 10(2), p. 204. doi: 10.3390/en10020204.

Wulveryck, M. (2000). Contrôle de courants alternatifs par correcteur résonnant multifréquentiel: application à la commande de systèmes électrotechniques non linéaires." Lille 1 No : 00 LIL1 0062., p. thèse de Doctorat. Université des Sciences et Tech.

Ye, T., Dai, N., Lam, C.-S., Wong, M.-C. and Guerrero, J. M. (2016). Analysis, Design, and Implementation of a Quasi-Proportional-Resonant Controller for a Multifunctional Capacitive-Coupling Grid-Connected Inverter. IEEE Transactions on Industry Applications, 52(5), pp. 4269–4280. doi: 10.1109/TIA.2016.2581152.

Zhao, J., Jing, W. and Wang, J. (2018). An Indirect Optimization Scheme for Tuning A Fractional Order PI Controller Using Extremum Seeking. Mechatronics, 56, pp. 146–156. doi: 10.1016/j.mechatronics.2018.11.003.

Zmood, D. N. and Holmes, D. G. (2003). Stationary Frame Current Regulation of PWM Inverters with Zero Steady-State Error. IEEE Transactions on Power Electronics, 18(3), pp. 814–822. doi: 10.1109/TPEL.2003.810852.

Appendix

Quantity	Symbol and magnitude
Rated Power	Pn = 5.5 kW
Rated voltage	Vn = 110 V
Rated current	In = 6 A
Rated speed	Nn = 950 rpm
Number of poles	2*p = 6
Rated Frequency	f = 50 Hz
Stator resistance	Rs = 2.03 Ω
Rotor resistance	Rr = 3 Ω
Stator inductance	Ls =0.215 H
Rotor inductance	Lr = 0.215 H
Mutual inductance	M = 0.2 H
Moment of inertia	J = 0.06 kg.m^2
Coefficient of viscous friction	kf = 0.006 N.m.s/rad

Table A1. Dual star induction machine parameters